Tribol Lett (2009) 36:17–29
DOI 10.1007/s11249-009-9454-2

ORIGINAL PAPER

Failure Analysis and Condition Monitoring of an Open-Loop Oil System Using Ferrography

O. Levi · N. Eliaz

Received: 26 March 2009 / Accepted: 27 April 2009 / Published online: 12 May 2009

Abstract Condition monitoring of dynamic systems based on oil analysis is well known for closed-loop systems. The motivation for this work stemmed from repeating failures of Wankel engines. Failure analysis identified contact fatigue as the failure mechanism, but could not identify the cause. Thus, the objective of the work was to develop a method for condition monitoring of open-loop oil systems. A variety of analytical techniques was evaluated, including direct-reading ferrography, analytical ferrography combined with computational image analysis, atomic emission spectroscopy, and scanning electron microscopy combined with energy dispersive X-ray spectroscopy. Procedures for collection and separation of oil samples were developed. Analytical ferrography was found most useful in condition monitoring. Six engines were detected in their early failure stage. Those engines were disassembled, and contact fatigue failures in the bearing needles were observed. The quantitative image analysis allowed for a fairly objective rating of the wear level. The method developed in this work has already been implemented on a daily basis for monitoring the health of Wankel engines, with much success.

Keywords Aviation · Internal combustion engine oils · Ferrography · Failure analysis · Oil condition monitoring · Ferrous alloys, steel · Needle roller bearings · Abrasive wear · Rolling-contact fatigue · Wear particle analysis

O. Levi · N. Eliaz (✉)
The Materials Science and Engineering Program & School of Mechanical Engineering, Tel-Aviv University, Ramat-Aviv, Tel-Aviv 69978, Israel
e-mail: neliaz@eng.tau.ac.il

O. Levi
The Failure Analysis Department, Materials Division, Depot 22, Israel Air Force, P.O. Box 02538, Tel Aviv, Israel

1 Introduction

Lubricated machines are usually characterized by three regimes in their wear rate versus time ("Bathtub") curve: wearing-in (running-in), normal (stationary), and severe (abnormal) wear [1]. Different types of wear result in generation of wear particles with different shapes, sizes, surface morphologies and colors [2–6]. Rubbing particles, for example, are typical of abrasive wear. Spalling particles, on the other hand, are associated with fatigue wear. Surface fatigue wear, also known as rolling contact fatigue, occurs predominantly in rolling element bearings. The four typical types of wear particles associated with this wear mechanism are micro-spall, laminar, chunky and spherical particles.

Condition monitoring is the process of monitoring a parameter of condition in machinery, such that a significant change is indicative of a developing failure. It is a major element of predictive maintenance. The use of condition monitoring allows maintenance to be scheduled, or other actions to be taken, in order to avoid the consequences of failure, before it occurs [1]. Different condition monitoring techniques have been suggested for aircraft components [7–10]. Condition monitoring based on oil analysis is well established [11–15]. Spectrometric oil analysis program (SOAP) is used for predictive maintenance in many closed-loop lubricating systems. Atomic emission spectroscopy (AES) is a diagnostic maintenance tool used to determine the type and amount of wear metals, additives and contaminations in lubricant fluid samples. The presence of unusual concentrations of elements in the fluid sample can indicate abnormal wear. Spectrometric analysis is limited to particulate contamination with size of 10 μm or less; larger contaminations are overlooked. Thus, the detection efficiency of spectrometric oil analysis decreases as the

wear particle size increases. In the system studied in the present work, no filters exist in the outlets. Therefore, large wear particles may be found in oil samples, thus requiring the use of other analytical techniques.

1.1 Ferrography

Ferrography is an example of condition monitoring technique, which has been found very sensitive and successful in monitoring the wear state of engineering systems, including in aeronautical and aerospace applications. This is a method of particle separation onto a glass slide based upon the interaction between an external magnetic field and the magnetic moments of the particles suspended in a flow stream [15, 16]. The method was developed by Westcott et al. in the early 1970s to investigate the occurrence of wear particles in lubricated dynamic components [17–21], and is used either as the primary analytical method or in conjunction with spectrometric analysis [1, 13].

In ferrographic examination, four types of ferrographs may be used. The direct-reading (DR) ferrograph uses optical density to quantitatively measure the concentration of wear particles in a lubricating oil or hydraulic fluid [12, 21, 22]. A powerful magnetic-gradient field causes particle deposition into a glass precipitator tube, in descending order of size. Light attenuation at two locations along the path—at the entry deposit (D_L, particles larger than 5 μm) and at a point several millimeters farther down the tube (D_S, particles smaller than 5 μm)—is used to quantify the relative concentration D_L/D_S of particles. An increase in the D_L value indicates that the system has entered into an abnormal wear mode. Values of wear particle concentration (WPC) and the percent of large particles (PLP) are thereby derived, establishing machine wear baselines and trends in wear condition [1]. When an abnormal wear mode is detected, analytical ferrography is used for more in-depth analysis.

The second type of ferrograph, which provides more valuable information, is called "analytical ferrograph". In analytical ferrography, a ferrogram (i.e. microscope slide with deposit of captured particles) is prepared by pumping a fluid sample (e.g. oil or diluted grease) that contains wear particles through Teflon tubing. The sampling procedure in the field has significant effect on the validity of the results. The ideal sample is taken immediately downstream from the lubricated surfaces. The pumping is onto a specially prepared glass substrate, which has a non-wetting barrier painted on one surface to centrally channel the liquid. The ferrogram is slightly tilted, with the entry end elevated, so that the fluid flows downward within the barrier toward a waste bottle. The tilted ferrogram is mounted above two permanent magnets. The magnets are separated with their magnetic poles counterposed, so that a strong magnetic field gradient is created in the vertical direction above an Al strip. Ferrous particles in the fluid experience a strong downward force. These particles migrate through the fluid down to the glass surface, where they are deposited in strings perpendicular to the direction of fluid flow. Because the distance from the magnet to the substrate is slightly greater at the entry side than at the exit side, the magnetic field strength is weaker at the entry side, causing only the largest (magnetically affected) particles to deposit. Farther down the ferrogram, the progressively stronger magnetic field deposits progressively smaller particles. For the same particle shape, motion downwards through the fluid as a function of size is governed by the ratio of the particle diameter cubed to the particle diameter squared. Nonferrous particles and contaminants travel downfield in a random distribution pattern, not being oriented by the magnetic field. They often appear between the strings of ferrous particles. Contaminants, such as sand and dirt, fibers and friction polymers, are also distributed in an irregular fashion throughout the length of the slide. After all the fluid in a given sample has been run across the ferrogram, a fixer solution is run to remove residual fluid. After the fixer dries, the ferrogram is ready for observation under the microscope. This is often a special microscope, equipped with both filtered-red reflected and filtered-green transmitted light sources that may be used simultaneously. This lighting scheme, called bichromatic illumination, will show a metal as red and a non-metal as green. Chemical analysis of wear particles can be carried out by various analytical techniques. Heat treatment of the particles on the ferrogram is another quick, inexpensive method of identification. By quantifying the ferrographic patterns (i.e. number, shape, size and texture) and determining the composition of different particles on the ferrogram, the origin, mechanism and level of wear can be determined [1]. A Wear Particle Atlas was constructed, providing information for the identification of various wear particle types, the description of wear modes that generate these particles, and as a guide to the prediction of machine operating condition based on the identified modes [2]. Since then, several new atlases have been published, some of which in electronic format. Machine maintenance records should suggest a proper sampling frequency. Once a possible problem is detected, the sampling frequency must be increased, until a positive determination is made on machine condition and the action to be taken. For each lubricant parameter that is measured, a control record is built that, after a period of time, will reveal normal operating ranges for a given type of machine/lubricant [1]. Analytical ferrography has been applied in the Israel Air Force with great success to monitor the health of helicopter gearboxes [1].

The third type of ferrograph is the on-line ferrograph [23–27]. The fourth type of ferrograph is bio-ferrograph. This is a recent modification of the conventional ferrograph. It was specifically developed to allow for magnetic isolation of target cells or tissues [28–33]. These two types, however, are outside the scope of this article.

1.2 The Wankel Engine

In this work, failure analysis and condition monitoring of Wankel engines were carried out. This is a specific type of internal combustion engine that belongs to the single-rotary piston family and is based on a thermodynamic cycle equivalent to that in a four-stroke engine: intake, compression, work/expansion and exhaust [34, 35]. The concept of rotary engine was invented by Felix Wankel during World War I. Figure 1 shows part of a Wankel engine that failed. A triangular rotor rotates on an eccentric shaft and gets its motion contour due to wheeling on the stationary gear. Because the rotor and the shaft are not rotating at the same velocity, there is a needle bearing between them. The forces, which are transported to the shaft, pass through the needle bearing. The bearing must be strong enough in order to avoid failure while passing the force. The purpose of the oil system is to lubricate the main rotor bearings, eccentric shaft bearing (needle bearing) and main seals.

The oil system in this engine is an open-loop system (i.e. the oil flows through the parts only once and is disposed rapidly into the atmosphere). Figure 2 illustrates the oil route. The oil pump pumps the oil from the tank and flows it through four channels: (1) rotor housing (drive side), (2) fan bearing, (3) rotor bearing, and (4) return port (unused oil). The oil from channel 1 burns with the fuel. The oil from channel 4 returns to the oil tank. The oil from channel 2 flows through the needle bearing and is mixed with the oil from channel 3 at the outlet of the air-cooling system. There, oil from channels 2 and 3 is ejected to the atmosphere as spray. This spray was the source of oil samples in

Fig. 1 A Wankel engine that failed

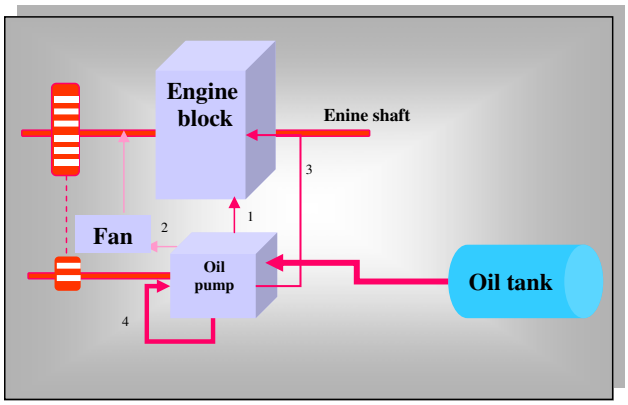

Fig. 2 The oil route in the Wankle engine studied in this work

the present work. To the best of our knowledge, this is the first time that such an analysis of an open-loop oil system is used for condition monitoring. In contrast to the case of helicopter gearboxes, no maintenance manual and definition of baseline are available with the system's manufacturer.

The motivation for this work stemmed from repeating failures of Wankel engines. During an engine operation, failure occurred and the engine ceased operating. Black oil was found at the air outlet and low compression values were measured. Similar events occurred in three other engines. It was hypothesized that oil analysis may aid in monitoring the condition of the engine, although it is an open-loop oil system. Thus, the objective of this work was to develop an analytical method for condition monitoring of open-loop systems. The Wankel engine served as the case study. A by-product of this work may be extension of the use of ferrography to new applications that have not been explored before.

1.3 The Challenges in Ferrographic Analysis of an Open-Loop Oil System

A closed-loop system typically relies upon an analog electronic control unit and an oxygen sensor, which is installed in the exhaust, and maintains a consistent air-to-fuel ratio. Open-loop systems raise higher demands for maintenance and produce higher levels of emissions than closed-loop systems. Generally speaking, due to accumulation of wear particles with time in closed-loop systems, the concentration of wear particles in these systems is expected to be higher than in open-loop systems. In the latter systems, the timing of lubricant sampling and its duration may have significant effect on the measured concentration of wear particles.

At an early stage of the project, several doubts made it of high risk. Firstly, to the best of our knowledge, no ferrographic analysis of an open-loop oil system has been

reported to date, possibly due to the assumption that most of the wear particles are lost. Secondly, there was no idea whether the oil spends sufficient time near the needles bearing to allow capturing of enough particles for meaningful analysis. Thirdly, there was no idea whether the rate of particle removal from the surface of parts was sufficiently high compared to the rate of oil flow and the duration of oil sampling at the air outlet. Fourthly, assembly of a collecting tool with high efficiency at the air outlet could disturb the air flow, thus raising the engine temperature, with possible damage to the engine. The decision of the right time for oil sampling was complicated. It was assumed that when sampling oil from a cold engine (i.e. that has just been ignited), particles related to the ignition and to the initial rubbing may deposit on the particles generated during failure, thus masking them. On the other hand, waiting too much before sampling was impractical because the system could not be in use for other purposes while being monitored. It also involved time consumption and economical aspects, which could make the new method less attractive. Finally, the optimal set of lab tests should be defined in order to construct meaningful results, in the most efficient and cost-effective manner.

2 Materials and Methods

Inspection by naked eyes was carried out both during failure analysis and during disassembly of the core parts. Stereomicroscopic examination was also carried out, using Wild Heerbrugg M8 stereomicroscope. Scanning electron microscope (SEM, JEOL model JSM-840A) was used both for observing the wear damage at the needles and for fractography. Energy dispersive X-ray spectroscopy (EDS) was used to verify the chemical composition of the materials in the core parts during failure analysis, as well as for chemical analysis of the debris filtered from the oil samples. To this aim, a Link ISIS 300 EDS system from Oxford was used. Hardness tests were done on metallographic cross-sections, within the bulk material of the needles, rotor bushing and shaft, by means of the Vickers method and a mass of 10 kg. A V-100A hardness tester from Leco was used. Micro-hardness tests were also carried out in order to profile the hardness values across the hardened layer of the shaft. The micro-hardness values were measured on metallographic cross-sections by means of the Vickers method and a mass of 200 g, using micro-hardness tester model 1600-6400 from Buehler. Metallographic cross-sections were prepared in order to analyze both the microstructure and cracking path in the failed parts. The inspections were done using a light microscope model MeF3 from Reichert-Jung.

Analytical ferrography was applied to mixtures of oil with IGX solvent (CCl_2FCH_3), using Dual Ferrograph Analyzer from Standard Oil Instrument Technologies. Microscopic evaluation was carried out by means of Ferroscope IV CH2 from Olympus Optical. A DR-Ferrograph 720700 from Predict Technologies was also used. AES was done to determine the weight-concentration (ppm) of different elements in the oil sample. A rotating disc emission (RDE) Spectroil M spectrophotometer from Spectro was used.

In the framework of this project, a new atlas of wear particles was constructed for the specific system. Thus, it became necessary to correlate the microscope images with the engine condition (level of wear), reliably and accurately, in a non-subjective manner. Basic quantitative image analysis of wear particles [36, 37] was done on light-microscope images of ferrographs, using Adobe Photoshop CS program ver. 8.0. Two parameters were actually measured: coverage (total area) and area fraction of the "black" rubbing particles and of the shiny spalling particles. The procedure included selection of 400 × 500 pixel pictures, sampling of the color to be analyzed, obtaining the number of pixels the color chosen covers, and selecting two Fuzziness numbers for comparison.

3 Results and Discussion

3.1 Initial Failure Analyses

As mentioned in Sect. 1.2, the motivation to this work stemmed from failures of four Wankel engines. Black oil was found at the air outlet. As neither new oil nor used oil exhibits a similar color, the origin of such black color may be either burnt oil or the presence of many black particles in the oil. Because the operation times of the four engines were different (174, 18, 115 and 22 h, for engines 1 through 4, respectively), the failure could not be related to either the wearing-in or the severe wear regimes. Visual inspections of the rotor bearing revealed similar findings after disassembling the engines. The needles in the rotor bearing were found thinner than their initial size. Figure 3a and b demonstrates the condition of the needles observed in the first and third failure events, respectively. In Fig. 3a, the top four needles are from the failed engine, while the lower two are new, reference ones. Several needles from the third event were found broken (Fig. 3b).

Geometrical measurements revealed that the diameters of the needles in all failure events decreased by 0.25–0.5 mm. This alone could explain improper operation of the engine. The needles became non-uniform in shape, as evident in Fig. 4. New needles have non-sharp edges in order to concentrate the loads around the center of the

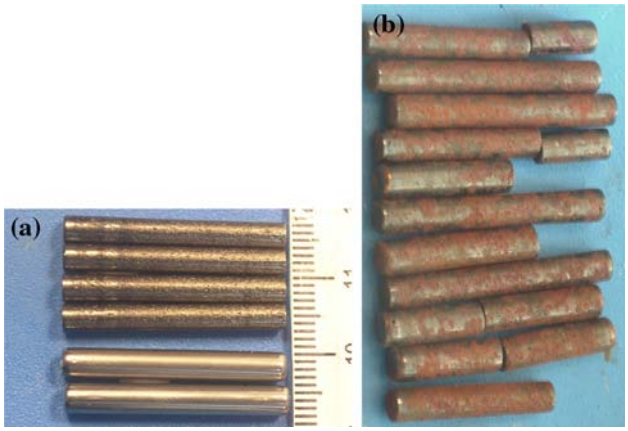

Fig. 3 Needles from the first (**a**) and third (**b**) failure events

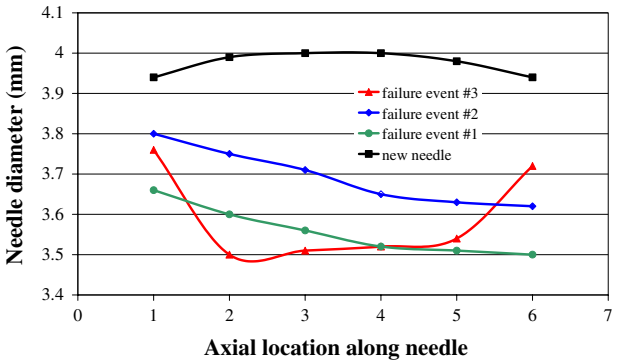

Fig. 4 The change in the rotor bearing's needle diameter in new versus failed needles

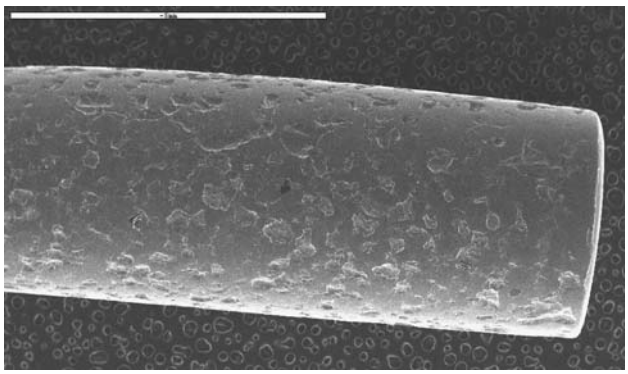

Fig. 5 SEM image of the surface of a needle from the first failure event. Scale bar: 5 mm

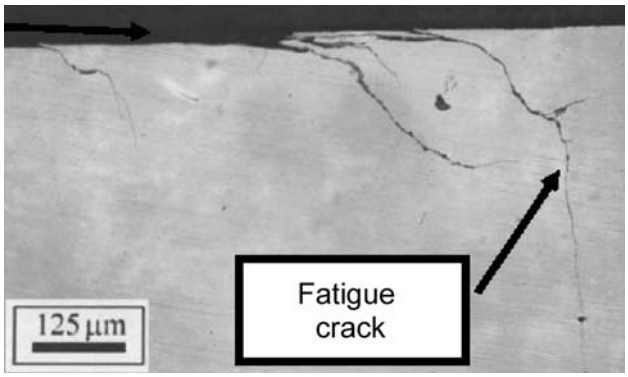

Fig. 6 Light microscope image of the metallurgical cross-section of a needle from the first failure event

longitudinal axis of the needle. The needles from the first event had cone shape, with the diameter decreasing gradually from 3.66 mm at one side to 3.5 mm at the other side. A similar phenomenon was discovered in needles from the second event, with the diameter varying from 3.85 to 3.7 mm (side to side). The third event resulted in bone-like needles, i.e. maximal decrease in diameter (down to 3.45 mm) around the center of the needle. In comparison, new needles are characterized by a uniform diameter of 3.989–3.991 mm. In Fig. 4, the different shape of curves in the case of failure events #1 and #2 compared to #3 is associated with different failure scenarios, as suggested later in this section.

The material composition (EDS) and hardness were characterized as alloy steel AISI 52XXX and 58–60 R_C, respectively, as required in the manufacturing drawing. Stereomicroscopy revealed many pits on the needle's surface. Figure 5 shows a low-magnification secondary electrons SEM image of a needle from the first event. Pits, typical of spalling, are evident on the surface. Metallurgical cross-section of a needle from this event revealed cracks emanating at the subsurface (Fig. 6). Such subsurface cracks are characteristic of a contact fatigue mechanism [38] and could result in removal of flaked particles from the surface. Contact fatigue is common in bearings and rolling parts under loads. This failure mechanism is associated with Hertzian contact (shear) stresses that are maximal at the subsurface [39]. Therefore, cracks are initiated at the subsurface and propagate toward the outer surface. The final stage is removal of a particle from the material. As this is a time-dependent failure mechanism, sufficient time may exist for condition monitoring.

Visual inspection of the rotors from three failure events revealed clusters of pits adjacent to the drive side of the rotor bushing, radial cracks at identical distances along the circumference of the bushing, and excessive wear on the upper side of the rotor faces. The pits on the rotor surfaces (Fig. 7) seemed visually similar to those observed on the needles. Thus, it was concluded that the rotors failed in the same contact fatigue mechanism. Geometrical investigation showed an enlargement of the bushing inner diameter. Measuring the inner diameter along the bushing axis, from the drive side to the non-drive side, it became evident that the maximum enlargement was at the drive side.

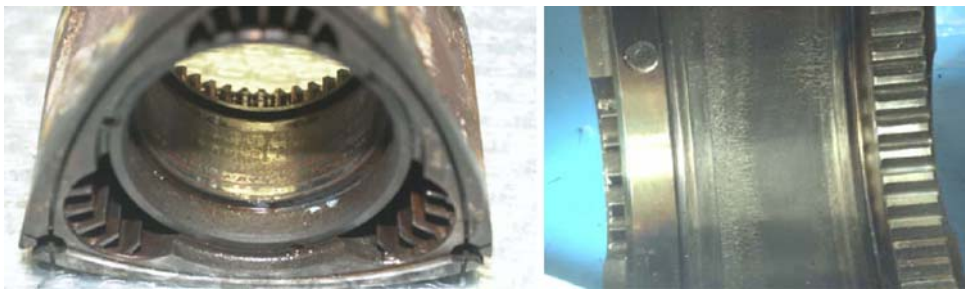

Fig. 7 Typical pitting on the internal circumference of the rotor

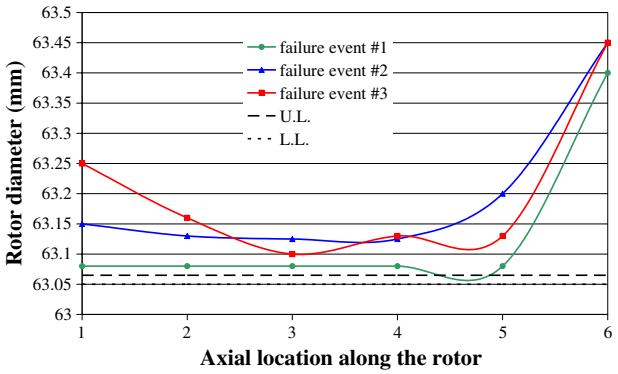

Fig. 8 Variation of the inner diameters of the rotors bushings from three failure events, in comparison to the lower limit (L.L.) and upper limit (U.L.) in the manufacturing drawing

Fig. 9 The shaft with eccentric element from the first failure event (*middle*), a used item (*top*) and a new item (*bottom*)

Figure 8 presents the variation in the inner diameter of three bushings from the failure events. The upper limit (U.L.) and lower limit (L.L.) specifications in the manufacturing drawing are also shown in this figure, to illustrate the enlargement. The different shape of curves for failure events #1 and #2 compared to #3 is related to the different shape of curves in Fig. 4 and to different failure scenarios, as suggested below.

The shaft has an eccentric element, on which the rotor bearing rotates. The outer diameter of the eccentric element is the surface loaded by the engine operation through the rotor and the needles bearing. Visual inspection of the eccentric elements in the shaft revealed evidence of exposure to high temperature (upper and middle shafts in Fig. 9) and material removal from the surface (Fig. 10). Geometrical measurements showed no change in the outer diameter of the eccentric element compared to the upper and lower limits specified in the drawing.

The chemical composition and micro-hardness of the shaft material matched the drawing requirements. Yet, it should be noted that some time before failures started to occur, the manufacturer changed the design and raised the hardness requirement from 60 R_C to 66–67 R_C. The rationale was to reduce distortions. However, Zaretsky et al. [40] found that the maximum fatigue life and load capacity of rolling-element bearings made of SAE 52100 steel was achieved when the rolling elements were 1–2 R_C harder than the inner race. Thus, the increase of hardness in the design could be related to the sudden increase in the occurrence of failures.

Visual inspection of the stationary gear in the first failure event revealed severe wear of the teeth and a circumferential crack at the step (see arrow in Fig. 11). Fractography revealed fatigue crack with multiple origins on the inner radius, propagating toward the outer surface. In some places the crack propagated through the oil holes. Geometrical characterization revealed that the inner radius was much smaller than that specified (0.1 mm vs. 1 mm, respectively). All other dimensions were within the requirements.

Based on the results of the failure analyses described above, the following scenario was suggested for the development of failure. Due to a problem associated with the change of design, high Hertzian loads developed, leading to contact fatigue of the rolling elements (needles) and release of spalling particles to the races. Due to high friction, the temperature was raised and the hardness of the rotor bushing material decreased. With time, the outer diameter of the needles decreased, and the outer diameter of the bushing increased. Thus, loss of clearance occurred at the core, and the stationary gear started to be overloaded. Consequently, a fatigue crack was initiated at the outer diameter of the gear and the rotor outer faces contacted the housing. This, in turn, led to reduction in the engine's compression and to its turn-off (failure event #3 in Fig. 4). Alternatively, improper inner diameter could result in

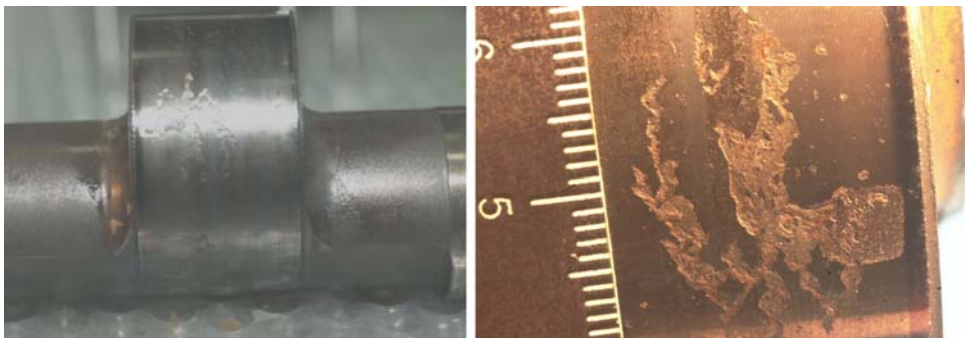

Fig. 10 Matter removal from the outer surface of the eccentric element

Fig. 11 Crack propagating in the gear from the first failure event

initiation of a crack at the inner circumference, tearing of a piece of metal, which entered the transmission, leading to fracture of the housing and engine's turn-off (failure events #1 and #2 in Fig. 4). Even if any of these scenarios actually had happened, the root cause of failure initiation was still ambiguous. However, taking into account also the structure and mode of operation of the Wankel engine, it was hypothesized that any wear particles could be contained in the oil until it reached the air outlet. If so, analysis of this oil may provide some valuable insights about the condition of either specific parts of the engine or the assembly. Different parts in this engine are made of markedly different materials (e.g. the bearing from AISI 52100, the stationary gear from AISI 4340, the rotor bushing from AISI 8620, the main shaft from Nitralloy, the end plates from Al casting, the rotor housing with Ni plate, the apex and side seals from AISI 1XXX). Thus, unambiguous identification of needles failure based on chemical analysis of wear particles may be possible.

3.2 Feasibility Tests

In one of the three failure events, the black oil was analyzed at the air outlet. EDS analysis of the debris separated from that oil revealed that they were made of AISI 41XX, AISI 521XX and AISI 87XX/86XX. In contrast, oil samples collected at the air outlet from more than three other systems that had not failed revealed only debris made of AISI 1XXX, and even then—only in one case. Therefore, it was concluded that it may be possible to identify the debris that reach the air outlet, at least in the last stage of failure. Hence, a question was raised, whether such data were satisfactory in order to assure a sufficiently early alert before failure.

3.3 Oil Sampling

A mechanical tool was designed in accordance with the following principles: (1) collect most of the particles that are contained in an air–oil–particles spray, and (2) do not influence the engine operation (e.g. by raising its temperature). The tool was assembled, prior to engine operation, onto the engine case at the air outlet. The following oil sample handling was developed:

1. Stir the bottle of the oil sample to obtain a homogeneous sample.
2. Wait 10 min in order to allow wear particles larger than 10 μm to concentrate at the bottom. These values were determined based on preliminary tests.
3. Collect 1 cm^3 oil from the top half of the bottle.
4. Collect 1 cm^3 oil from the bottom for EDS analysis.
5. Collect 2 cm^3 oil for Analytical Ferrography and 2 cm^3 oil for DR-Ferrography from the bottom of the bottle.

First, 15–20 cm^3 oil was collected in 35 min from a cold engine (i.e. without pre-running) that was run at 5500 rpm. This engine had 174 operation hours. Visually, the oil was dark, and few particles could be noticed. EDS analysis was carried out on a 2 cm^3 sample. Particles could be assigned with the following chemical compositions: AISI 52XXX, AISI 1XXX, AISI 41XX, Fe–Cr and Al 5XXX/6XXX. All except the latter could be related to specific parts of the engine, while the latter was ascribed to the mechanical tool. Second, a comparison was made between an engine in the cold condition versus the hot condition. A decrease in the number of particles was observed in the hot condition. Yet, the overall number of wear particles was too low ($\leq$21) to provide meaningful condition monitoring. Thus, it

Table 1 DR-Ferrography analysis of the oil in a Wankel (#5)

	Sample #1	Sample #2	Sample #3
WPC	87	58	61
D_L	56	36	40
D_S	30	21	21

was concluded that either the sampling duration should be increased, the engine should run at a higher rpm value, or the EDS analysis should be omitted from the protocol. In an attempt to avoid long interrupt of the regular operation of the engine, and due to financial constraints, the third option was selected.

AES of oil samples from two engines after three samplings that were collected at constant time intervals revealed that, for most elements, the concentrations of Fe, Ni, Al and Ag were highest in the first sample. These results were supported by DR-Ferrography data (Table 1). It was assumed that the higher concentrations of these elements in the first sample resulted from rubbing of the interfaces in the core element of the cold engine. Therefore, the following oil samples were acquired several minutes after an initial 10-min run process.

3.4 The First Batch of Condition-Monitored Wankel Engines

As a first trial, nine engines with different operation times were sampled in accordance with the method described above. The Fe, Al and Ag concentrations obtained from AES, the WPC and D_L/D_S values obtained from DR-Ferrography, and the levels of spalling and rubbing determined based on Analytical Ferrography via comparison to a commercial atlas of wear particles are shown in Fig. 12.

The WPC curve in Fig. 12 is similar in shape to the Bathtub Curve. The D_L/D_S curve shows that the relative density of large particles is more dominant in the engine at an early stage of operation and then declines in engines with longer operation times. It is anticipated that if more engines with even longer operation times would have been analyzed, the ratio D_L/D_S would increase again. The concentration profiles of Fe, Al and Ag have some similarity to the profile of the WPC curve.

Two engines in Fig. 12 should be farther explained, namely the 4th and the last one. The 4th engine disturbs the monotonic behavior; the WPC, D_L/D_S, rubbing and spalling levels are quite high compared to their adjacent engines. This may indicate an irregular engine behavior. The last engine behaves as expected, except the drop in the concentration of Fe. This means that, while the WPC curve indicates an increase in the number of ferrous particles, the concentration of iron decreases. These results may be

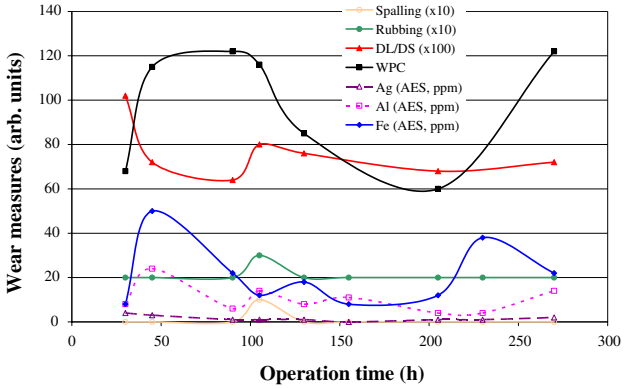

Fig. 12 AES, DR-Ferrography and Analytical Ferrography data collected from the first batch of nine Wankel engines with different operation times. The AES values are given in wt. ppm units. The spalling and rubbing levels (Analytical Ferrography) are rated as either 0 (no damage), 1 (low), 2 (moderate) or 3 (severe) and then multiplied by 10 for graphical presentation. Similarly, the D_L/D_S ratio was multiplied by a factor of 100

explained in terms of the detection limit of AES, which cannot detect particles larger than 10 μm. Based on the results from the first batch of engines, it was concluded that the method developed was adequate, and that the oil sampling could be extended to monitor the health of the whole fleet.

3.5 Condition Monitoring of the Whole Fleet

In this stage, each engine was sampled every 30 h (see Sect. 3.3). When any indication for an increase in wear level was suspected, the sampling interval was narrowed. Because no maintenance policy existed, each suspected indication led to a specific status discussion. The abnormality was defined in comparison to the results acquired for other engines with similar operation times. As time elapsed, the definition of "normality" became clearer and characteristic values could be defined. A database was constructed for all engines, based on AES, DR-Ferrography and Analytical Ferrography data.

Figure 13 summarize AES, DR-Ferrography and Analytical Ferrography data of 8 of the 39 sampled engines. It should be emphasized that only eight engines are presented herein for graphical simplicity purpose only, and that they represent the whole population. The sampling numbers do not necessarily represent the same time intervals. During follow-up, two engines were identified as exhibiting irregular behaviors. These engines are marked as "A" and "B" in Fig. 13. The results of engine "A" were based on samplings at operation time intervals of about 30 h. Significant increase in wear indicators was evident. The AES-Fe value was within the range of 10–20 ppm for the first three samples, then increased sharply to 117 ppm, and

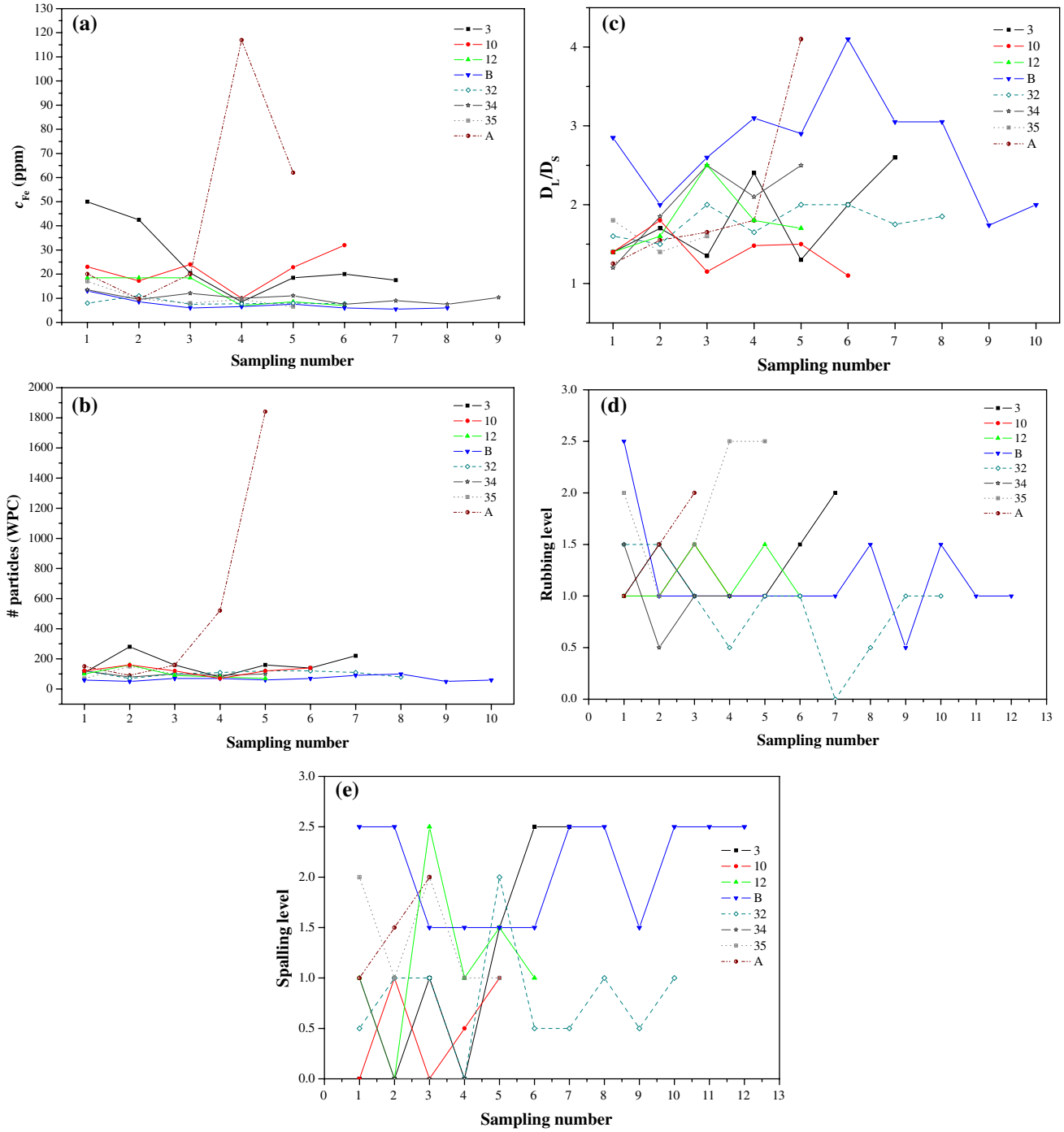

Fig. 13 Wear indicators measured for eight of the whole fleet. The sampling numbers do not represent constant time intervals. **a** Fe concentration based on AES, **b** WPC and **c** D_L/D_S values based on DR-Ferrography, **d** rubbing and **e** spalling rates based on Analytical Ferrography

finally declined to 62 ppm, which was still high compared to other engines. The latter decline may be attributed to formation of large particles, as explained in Sects. 1 and 3.4. The WPC indicator increased rapidly to nearly 2000, while the D_L/D_S value increased monotonically, from 1.25 to 4.1. The rubbing indicator increased gradually, while the spalling indicator was not as high compared to other engines. Analysis of the ferrogram revealed that rubbing wear occurred in this engine. This can explain the increase in both the size and the number of wear particles over time. Based on the collection of data, it was concluded that this engine ("A") behaved abnormally and experienced severe

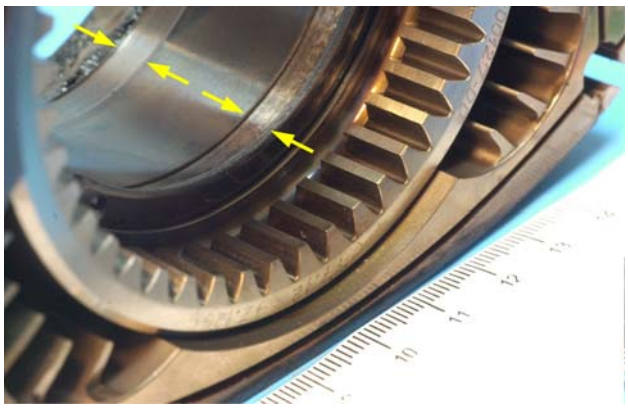

Fig. 14 Macroscopic view of abrasive wear in the rotor bushing of engine "A"

wear. Therefore, this engine was disassembled and carefully analyzed. Excessive wear was observed at the rotor bushing race, in the form of two wear strips near the bushing edges (see arrows in Fig. 14). This kind of failure is common in the Wankel engine, although usually not to this high level. The abrasive wear damage in engine "A" was related to the needles cage of the main bearing. The cage geometry had salient shoulders at the edges, which probably rubbed the rotor bushing race due to the centrifugal forces acting on the cage. The eccentric movement of the core intensified this phenomenon.

Engine "B" was evaluated by 8–12 samples and behaved differently. The first 4–6 samples were collected while the engine was assembled on the system, whereas the remaining samples were acquired while it was on the running test facility. The Fe concentration values (AES) were consistently fairly low, with no significant difference between the two modes of operation. A similar behavior was observed for the WPC indicator. The D_L/D_S values for this engine were higher than for other engines; in the second mode of operation, the values decreased. Analytical Ferrography revealed higher level of spalling than rubbing. The spalling level remained high (mostly at 2.5, i.e. moderate/heavy) regardless of the mode of operation. After disassembling engine "B", no indication of excessive abrasive wear was found in any of the core elements. In contrast, flaking particles from the needles of the bearing were found. Those flaking particles were identified under a stereomicroscope as being related to contact fatigue (spalling). The findings were similar to those reported in Sect. 3.1, which actually triggered the development of the new condition monitoring process. A small amount of pits indicated that the failure was at its early stage. Combining the findings with those for engine "A", it may be concluded that the new method is sensitive and effective in identifying different wear mechanisms occurring in different core elements. It is also confirmed that AES is not useful for identifying large particles as those generated by contact fatigue. Another conclusion is that rubbing damage may be much easier to detect compared to spalling, as it was accompanied by increase in the values of more wear indicators. One obstacle in the case of rating spalling by Analytical Ferrography may be that the decision levels (none, few, moderate or heavy) were adapted from another system (transmission gear) and made by (somewhat subjective) evaluation of images. Consequently, the actual observation of low damage to the needles did not match the prediction moderate/heavy. Hence, it may be concluded that the decision level in Analytical Ferrography should be adjusted to the specific system under investigation.

The fleet continued to be sampled, and contact fatigue was detected in other six engines. Additional 400 samples were analyzed and presented graphically (not included herein). Most of the data were confined within a fairly narrow range. Normal levels (baseline) could be defined as a maintenance policy. Assuming a normal distribution, the averages and standard deviations were calculated and tabulated. Based on this data, $\bar{X} + 2\sigma$ was found more appropriate than either $\bar{X} + \sigma$ or $\bar{X} + 3\sigma$, where $\bar{X}$ is the mean value and σ is the standard deviation, for predictive maintenance purposes.

3.6 Quantitative Image Analysis and Rating of Wear Particles

In this work, the damage level was rated according to four levels: 0 = none, 1 = few, 2 = moderate, and 3 = heavy, based on light microscope images acquired in the framework of Analytical Ferrography. These levels were adapted from an atlas of wear particles in transmission systems, the pictures in which were also used as a reference. The intermediate levels 0.5, 1.5 and 2.5 were added, arbitrarily. The procedure is similar to that of manually ranking the inclusion content of steels by comparison to standard Plates [41]. The rating in this work was based, in most cases, on the estimations of three different people. Figure 15 shows four typical images and the ratings that were assigned to them, both for rubbing and spalling particles.

In order to make the rating less subjective, quantitative image analysis was done as described in Sect. 2. Rubbing particles can be identified by their small dimensions and by their arrangement as strings oriented with respect to the magnetic field. It became evident that the dark particles in the images were indicative of rubbing wear. Spalling particles can be identified by their round contour, large size and very shiny appearance. They may also be arranged within strings. Therefore, measurements of the shiny level, roundness, particle size and coverage of the shiny area may be useful in quantitative image analysis.

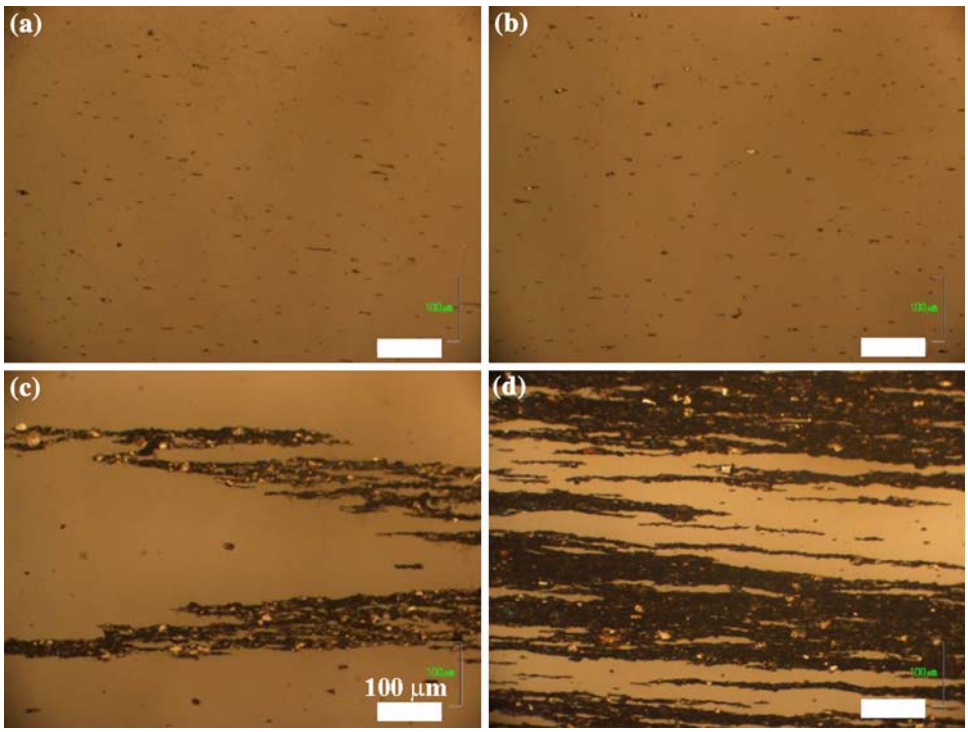

Fig. 15 Light microscope images (Analytical Ferrography) demonstrating different levels of wear. The following ratings were assigned subjectively: **a** rubbing 0.5, spalling 0; **b** rubbing 0.5, spalling 0.5; **c** rubbing 2, spalling 1.5; **d** rubbing 3, spalling 2. All white scale bars are 100 μm long

Table 2 Wear level ratings (rubbing and spalling) according to quantitative image analysis in comparison to a manual evaluation (reflected by the slide #)

The digits after "r" in the "Slide #" column reflect the level of rubbing, the digits after "s" reflect the level of spalling

Slide #	Rubbing level	Rubbing area fraction	Spalling level	Spalling area fraction
r05s0	0.5	0.6–1.4	–	–
r05s05	0.5	0.9–1.3	0.5	0.03–0.04
r1s05	1	3.3	0.5	0.03
r1s1	1	4.0–4.3	1	0.07–0.17
r15s1	1.5	5.0–9.5	1	0.16–0.18
r2s15	2	20.2–20.6	1.5	0.35–0.46
r25s2	2.5	32.1–35.0	2	0.27
r25s25	2.5	31.2–32.7	2.5	1.05
r3s2c	3	59.2–59.7	2	0.1–0.2

Table 2 summarizes the wear level ratings according to quantitative image analysis, in comparison to the more subjective rating described before. In most cases, the correlation between the two ways of rating is fairly good. Yet, it should be born in mind that the quantitative image analysis is almost not subjected to a personal bias and can be performed quite reliably by a single operator. Moreover, the quantitative image analysis did reveal two errors in the manual decision making: while the subjective method defined moderate spalling level for slides r25s2 and r3s2c, the quantitative image analysis indicated a lower spalling level. Re-evaluation supported the rating of the quantitative image analysis.

The lab tests used in this work dealt with monitoring the oil path in a dynamic system. Future work may be to compare the results to those obtained by other condition monitoring techniques such as vibration monitoring, temperature monitoring, or stress monitoring.

4 Conclusions

Based on the results presented in the paper, the following conclusions can be made:

- A sensitive, reliable procedure was developed for condition monitoring of an open-loop oil system, based mainly on Analytical Ferrography. The Wankel engine was used as case study. To the best of our knowledge, this is the first demonstration in the literature of the use of Analytical Ferrography for health monitoring of an open-loop oil system. The method is already used on a daily basis.

- A simple computational image analysis was found helpful in rating the wear (rubbing and spalling) in a more objective manner.
- A database was constructed and the baseline for normal wear condition was defined together with the most reliable statistical measure. This would be useful in future condition monitoring of the system.
- DR-Ferrography was found valuable to some extent (e.g. because of its simplicity), but did not provide the broad necessary view of the system.
- Atomic emission spectroscopy (AES) was found valuable only at a very early stage of failure because it overlooks wear particles larger than 10 μm. In some cases, it might have led to a misleading conclusion of normal instead of severe wear.
- Debris analysis by SEM/EDS was found worthless because it is applicable only to relatively large particles.
- One of the by-products of this work may be the extension of the use of ferrography to new applications.

Acknowledgments The authors are grateful to Mr. Kobi Basan and Mr. Konstantin Tartakovski for their significant contribution to the success of the project. We thank Mr. William Kopelovitch for his help in quantitative image analysis. We are also thankful to Prof. Isaac Garbar for his peer-review and professional advices.

References

1. Eliaz, N., Latanision, R.M.: Preventative maintenance and failure analysis of aircraft components. Corros. Rev. **25**, 107–144 (2007)
2. Bowen, E.R., Westcott, V.C.: Wear Particle Atlas (Revised), vol. 1. Naval Air Engineering Center Contract number N00156-74-C01682, July (1976)
3. Maslach, J.K.: Ferrographic analysis of grease-lubricated systems: an analysis of greases in roller bearings. Lubr. Eng. **52**, 662–666 (1996)
4. Toms, L.A.: Machinery Oil Analysis—Methods, Automation and Benefits, 2nd edn., pp. 106, 160. Coastal Skills, VA (1995)
5. Keith Mobley, R.: An Introduction to Predictive Maintenance, 2nd edn., p. 202. Butterworth-Heinemann, MA (2002)
6. Troyer, D., Fitch, J.: Oil Analysis—Basics, p. 67. Noria Corp., Tulsa, OK (2001)
7. Sheppard, K., Zagrai, A., Donskoy, D.: A non-linear acoustic, vibro-modulation technique for the detection and monitoring of contact-type defects, including those associated with corrosion. Corros. Rev. **25**, 81–96 (2007)
8. Calvello, G., Olin, S., Hess, A., Frith, P.: PHM and corrosion control on the joint strike fighter. Corros. Rev. **25**, 51–79 (2007)
9. Bovio, I., Lecce, L.: Health monitoring of aeronautical structures based upon vibration measurements and identification algorithms. Corros. Rev. **25**, 27–37 (2007)
10. Cajani, M.: Ageing airframes and corrosion maintenance. Corros. Rev. **25**, 263–274 (2007)
11. Ščekaturovienė, D., Višniakov, N.: Atomic emission spectrometric analysis in the assessment of wearing of vehicle engines. Mater. Sci. (Medžiagotyra) **10**, 15–17 (2004)
12. Doyle, E.D., Atkin, M.L.: A review and case study of wear mechanisms and condition monitoring. In: Joint National Symposium 1985: The Influence of Aviation on Engineering and the Future of Aeronautics in Australia, p. 23, Preprints, The Institution of Engineers, Melbourne, Australia (1985)
13. Stecki, J.S., Kuhnell, B.T.: Condition monitoring of jet engines. Lubr. Eng. **41**, 485–493 (1985)
14. Lukas, M., Anderson, D.P.: Analytical Tools to Detect and Quantify Large Wear Particles in Used Lubricating Oil. Spectro Inc., MA (2003)
15. Lockwood, F.E., Dalley, R.: Lubricant analysis. In: ASM Handbook Vol. 18: Friction, Lubrication, and Wear Technology, p. 302. ASM International, Materials Park, OH (1992)
16. Staff report, Ferrography: a tool for wear-particle analysis. Hydraulics & Pneumatics, November, pp. 59–61 (1986)
17. Seifert, W.W., Westcott, V.C.: A method for the study of wear particles in lubricating oil. Wear **21**, 27–42 (1972)
18. Westcott, V.C.: Method and apparatus for segregating particulate matter. US Patent 4,047,814, 13 Sept 1977
19. Reda, A.A., Bowen, R., Westcott, V.C.: Characteristics of particles generated at the interface between sliding steel surfaces. Wear **34**, 261–273 (1975)
20. Scott, D., Seifert, W.W., Westcott, V.C.: The particles of wear. Sci. Am. **230**, 88–97 (1974)
21. Roylance, B.J.: Ferrography—then and now. Tribol. Intern **38**, 857–862 (2005)
22. Stecki, J.S.: Failure prediction using ferrographic oil analysis techniques. In: Proceedings of the Conference on Lubrication, Friction and Wear in Engineering, p. 281. The Institution of Engineering, Melbourne, Australia (1980)
23. Merhib, C.P.: The on-line ferrograph. In: Proceedings of the Conference on Lubrication, Friction and Wear in Engineering, p. 277. The Institution of Engineering, Melbourne, Australia (1980)
24. Centers, P.W.: Laboratory evaluation of the on-line ferrograph. Wear **90**, 1–9 (1983)
25. Holzhauer, W., Murray, S.F.: Continuous wear measurement by on-line ferrography. Wear **90**, 11–19 (1983)
26. Barwell, F.T.: The role of particle analysis—a review of ferrography. In: Dowson, D., Taylor, C.M., Godet, M., Berthe, D. (eds.) Developments in Numerical and Experimental Methods Applied to Tribology, p. 3. Butterworths, London (1984)
27. Yan, L., Youbai, X., Fang, Z., Zhigang, Y.: Revision to the concept of equilibrium concentration of particles in lubrication system of machines. Wear **215**, 205–210 (1998)
28. Zhang, P., Johnson, W.P., Rowland, R.: Bacterial tracking using ferrographic separation. Environ. Sci. Technol. **33**, 2456–2460 (1999)
29. Zhang, P., Johnson, W.P.: Rapid selective ferrographic enumeration of bacteria. J. Magnetism Magnetic Mater. **194**, 267–274 (1999)
30. Johnson, W.P., Zhang, P., Fuller, M.E., Scheibe, T.D., Mailloux, B.J., Onstott, T.C., Deflaun, M.F., Hubbard, S.S., Radtke, J., Kovacik, W.P., Holben, W.: Ferrographic tracking of bacterial transport in the field at the Narrow Channel Focus Area, Oyster, VA. Environ. Sci. Technol. **35**, 182–191 (2001)
31. Meyer, D.M., Tillinghast, A., Hanumara, N.C., Franco, A.: Bioferrography to capture and separate polyethylene wear debris from Hip simulator fluid and compared with conventional filter method. J. Tribol. **128**, 436–441 (2006)
32. Parkansky, N., Alterkop, B., Boxman, R.L., Leitus, G., Berkh, O., Barkay, Z., Rosenberg, Yu., Eliaz, N.: Magnetic properties of carbon nano-particles produced by a pulsed arc submerged in ethanol. Carbon **46**, 215–219 (2008)
33. Ishay, J.S., Barkay, Z., Eliaz, N., Plotkin, M., Volynchick, S., Bergman, D.J.: Gravity orientation in social wasp comb cells

(Vespinae) and the possible role of embedded minerals. Naturwissenschaften **95**, 333–342 (2008)
34. West, K.C.: Energy Conversion, Brooks/Cole, p. 261. University of Tulsa (2000)
35. http://en.wikipedia.org/wiki/Wankel_engine. Accessed 3 May 2009
36. Raadnui, S.: Wear particle analysis—utilization of quantitative computer image analysis: a review. J. Tribol. Intern. **38**, 871–878 (2005)
37. Russ, J.C.: Computer-Assisted Microscopy: The Measurement and Analysis of Images. Plenum Press, NY (1990)
38. Powel, G.W., Mahmoud, S.E.: ASM Handbook Vol. 11: Failure Analysis and Prevention, 9th edn., p. 586. ASM International, Materials Park, OH (1986)
39. Lawcock, R.: Rolling-contact fatigue of surface-densified gears. Intern. J. Powder Metall. **42**, 17–29 (2006)
40. Zaretsky, E.V., Parker, R.J., Anderson, W.J., Reichard, D.W.: Bearing life and failure distribution as affected by actual component differential hardness. NASA Technical Note TN D-3101, Washington DC, November (1965)
41. ASTM E45-05e2: Standard Test Methods for Determining the Inclusion Content of Steel. ASTM International, West Conshohocken, PA